

DFT and Experimental Study of Electronic, Absorption and FT-IR Spectral Properties of Cu(II) Complex of Pyridine-Amide Ligand with Appended Ether Functionality

K. SHRIVASTAVA¹, D. DAS², B. KUMARI³ and P.P. DAS^{1,*} 

¹Department of Chemistry, Magadh University, Bodh-Gaya, Gaya-824234, India

²Department of Chemistry, School of Basic and Applied Sciences, Adamas University, Kolkata-700126, India

³Department of Chemistry, G.B.M. College, Gaya-823001, India

*Corresponding author: E-mail: parthapratimdasmu@gmail.com

Received: 24 September 2022;

Accepted: 17 November 2022;

Published online: 27 December 2022;

AJC-21086

The electronic structure, TD-DFT and FT-IR vibrational frequencies of copper(II) complex *viz.* [Cu(II)L₂], L = deprotonated form of *N*-(2-methoxyphenyl)benzamide] were investigated by DFT calculation and experimental studies. The optimized structure reveals distortion in the octahedral geometry of the complex. The magnetic orbitals, spin-density plot and orbitals involved in calculated electronic transitions from TD-DFT were all identified. Theoretical and experimental data were in comparable agreement.

Keywords: Copper(II) complex, *N*-(2-methoxyphenyl)benzamide, TD-DFT, FT-IR, DFT, Vibrational frequency, Spin-density plot.

INTRODUCTION

Carboxamide functionality is abundant in nature in primary structures of proteins and has biological significances [1]. Transition metal complexes of protonated/deprotonated pyridine/pyrazine-2-carboxamide ligands have always been rigorously studied over the years [2,3]. Their ability to form metal complexes with broad range of oxidations states due to their strong σ -donor property and variable geometry [4,5], along with interesting coordination properties are available both in literatures of coordination chemistry and bioinorganic chemistry [6]. As the lone pair on nitrogen is delocalized over the whole amide group, neutral ligands are commonly coordinated *via* carbonyl oxygen whereas, the deprotonated amide groups typically coordinate through amide-nitrogen atom. Quick and easy synthesis of both amide ligands and their metal complexes [5,7] have also been the reason for such extensive study. Over the years, scientists have included modifications in ligand structure, mainly if there's any linkage between two or more amide functionalities or addition of appended/peripheral donor sites. Such modifications alter the structure or properties/reactivities. Though their physical/spectrochemical properties are of interest for longer period now, but off-late study of their reactivity towards several catalysis reactions [4] and theoretical

aspects to support experimental findings have grown newer interest.

Metal complexes of pyridine/pyrazine amides have diverse activity and selectivity regarding these aspects [5]. The ease, with which the ligands' design can be changed using a modular strategy, is one aspect that makes them appealing for catalytic processes. By changing the amine framework and/or adding the appropriate functionalities to the pyridine nucleus, it is simple to change the electrical and steric characteristics. Theoretical support helps towards better understanding and better explanation with insights for obtained experimental results.

In this work, *N*-(2-methoxyphenyl)benzamide (HL) and its Cu(II) complex [Cu(II)L₂] in the deprotonated form (L) are the ligand and transition metal complex of significance. Thioether linkage [8] between two pyridine-2-carboxamide units in ligand is earlier reported in hexadentate environment. Framework with phenolate-O [9] or furan-O [10] is available but, appended ethers with pyridine/pyrazine-2-carboxamide in tridentate manner are rare in literature. Present aim in this work has been the rationalization of the finer picture of its electronic, structural and absorption spectral properties of the above complex by theoretical calculations. This will make it possible to compare the calculated results with experimental data, indirectly enhancing understanding of the matter. The

density functional theory (DFT) at the B3LYP level and time-dependent (TD)-DFT calculations for the same have been conducted.

EXPERIMENTAL

Computational programs: All DFT calculations were performed using the Gaussian 09 program with the B3LYP functional. Triple- ζ quality basis set (TZVP) was used for copper, nitrogen and oxygen, while SVP basis set was used for carbon and hydrogen. The TD-DFT calculations were performed employing the B3LYP functional and the polarizable continuum model, CPCM (CH_2Cl_2 as solvent). TD-DFT-derived electronic and FT-IR spectra were plotted using GaussSum. Corresponding orbitals and spin density plots were obtained using Chemcraft Visualization program.

Spectroscopic measurements were done by the following instruments: IR (KBr, 4000-600 cm^{-1}), Bruker Vector 22; Electronic, Perkin-Elmer Lambda 2 and Agilent 8453 diode-array spectrophotometer.

RESULTS AND DISCUSSION

The optimized structure of $[\text{Cu}(\text{II})\text{L}_2]$ is shown in Fig. 1. Selected bond lengths and bond angles are tabulated in Table-1. Cu(II) ion has utilized all possible coordination sites available from both ligands in tridentate mode and embraces distorted octahedral geometry, justified by bond angles. Bond lengths are in accordance with reported literature values of other Cu(II) complexes.

Absorption spectrum: Electronic spectrum of $[\text{Cu}(\text{II})\text{L}_2]$ was recorded in CH_2Cl_2 . The experimental UV-Vis spectra show a low intense peak at ~ 684 nm with $\epsilon \sim 225 \text{ M}^{-1} \text{ cm}^{-1}$, which clearly indicate crystal-field transition [11] (Fig. 2). Higher energy transitions at ~ 496 [$\epsilon \sim 6530 \text{ M}^{-1} \text{ cm}^{-1}$], ~ 380 [$\epsilon \sim 17850 \text{ M}^{-1} \text{ cm}^{-1}$] and ~ 345 nm [$\epsilon \sim 24725 \text{ M}^{-1} \text{ cm}^{-1}$] are ligand centred in origin [11,12]. The nature of ligand-based transitions was determined by TD-DFT calculations.

Magnetic susceptibility measurement: The magnetic susceptibility studies were carried out on both solid powdered and solution-state samples at room temperature to have an idea about the spin-state of the Cu(II) centre. The μ_{eff} values for solid-state and solution states were $1.84 \mu_{\text{B}}$ and $1.86 \mu_{\text{B}}$, respectively. This correspond to $S = 1/2$ spin-state. However to pinpoint, the same electronic structural aspects were theoretically studied too.

Electronic structural studies: Optimization of $[\text{Cu}(\text{II})\text{L}_2]$ reveals the closed-shell electronic configuration ($S = 1/2$). The optimization geometry reveals $+0.60$ spin density on copper, implying the spin state of Cu(II) centre (Fig. 3). The magnetic orbitals for $[\text{Cu}(\text{II})\text{L}_2]$ are displayed in Fig. 4. The singly occupied molecular orbital (SOMO; 134 α orbital) has $\sim 51\%$ Cu character.

TD-DFT studies: The absorption spectra of transition-metal complexes are by far the most difficult part to calculate *via* DFT. However, the TD-DFT results provide strong support for the experimental findings here (Table-2), which also predicted a transition at 665 nm of *d-d* origin, along with

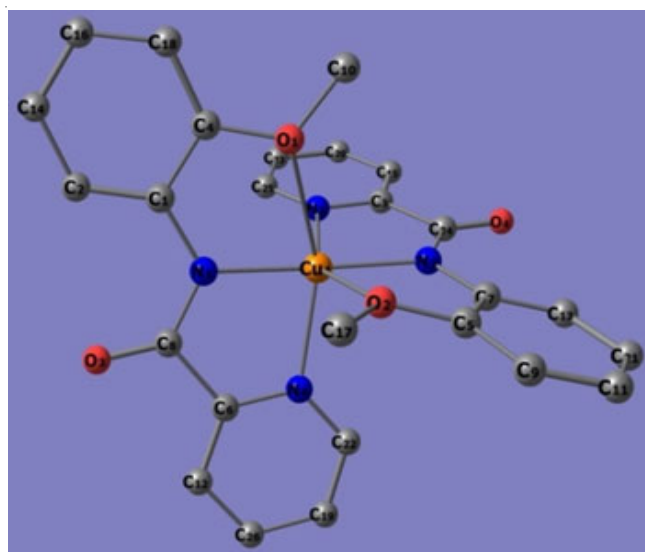
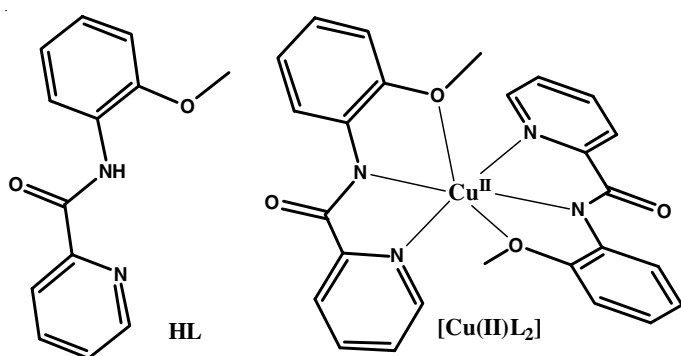
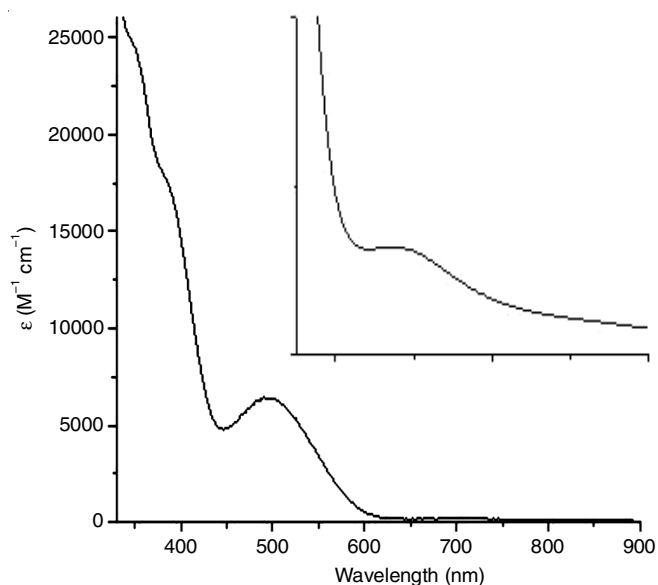
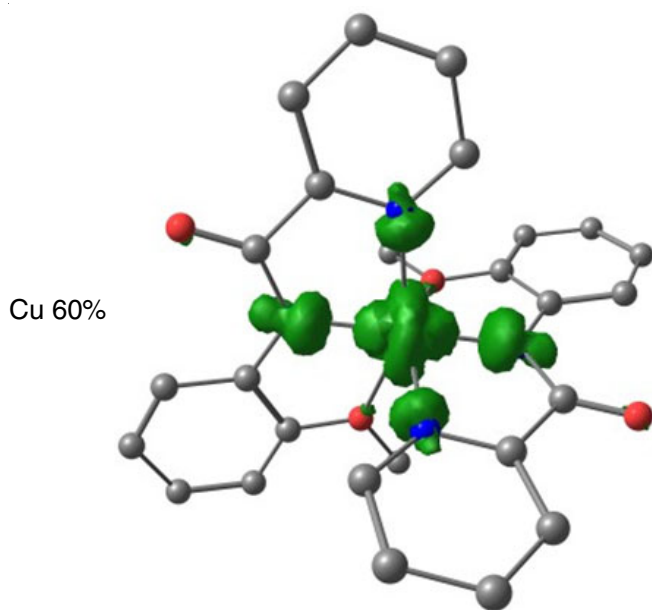
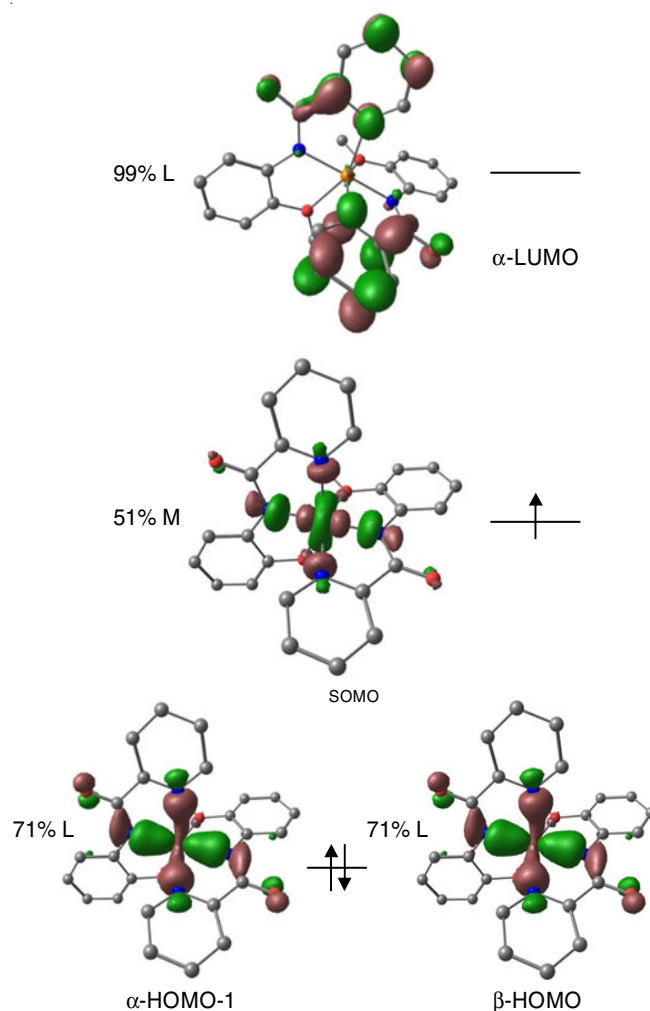


Fig. 1. Ligand frame work, complex $[\text{Cu}(\text{II})\text{L}_2]$ structure and DFT optimized structure of modelled complex $[\text{Cu}(\text{II})\text{L}_2]$

TABLE-1
SELECTED BOND LENGTH (\AA) AND BOND ANGLES ($^\circ$) IN OPTIMIZED STRUCTURE OF $[\text{Cu}(\text{II})\text{L}_2]$

Bond length (\AA)		Bond angle ($^\circ$)					
Cu-O1	2.36763	O1-Cu-O2	79.903	N1-Cu-N2	175.331	N2-Cu-N4	101.046
Cu-O2	2.36867	O1-Cu-N1	74.551	N1-Cu-N3	101.206	N2-Cu-O2	74.518
Cu-N1	1.98248	O1-Cu-N2	101.824	N1-Cu-N4	81.494	N3-Cu-N4	112.792
Cu-N2	1.98228	O1-Cu-N3	88.796	N1-Cu-O2	101.744	N3-Cu-O2	150.605
Cu-N3	2.12794	O1-Cu-N4	150.556	N2-Cu-N3	81.496	N4-Cu-O2	88.624
Cu-N4	2.12810						

Fig. 2. UV-Vis spectrum of $[\text{Cu}(\text{II})\text{L}_2]$ in CH_2Cl_2 Fig. 3. Spin-density plot of $[\text{Cu}(\text{II})\text{L}_2]$ Fig. 4. Magnetic orbitals of $[\text{Cu}(\text{II})\text{L}_2]$

transition at 495 nm (Fig. 5), pinpointed to be LMCT involving amide to metal, phenyl ring attached to amide to metal and amide and phenyl ring attached to amide to metal. Higher energy transitions at 321 and 369 nm are associated with intraligand charge transfer between amide and phenyl ring attached to amide to pyridine mainly. The calculated absorption spectra closely resembles the experimentally results.

TABLE-2
TD-DFT CALCULATED ELECTRONIC TRANSITION OF $[\text{Cu}(\text{II})\text{L}_2]$

Excitation energy (eV)	λ (nm)	f	Transition	Character
1.86	665	0.0040	$\beta\text{-H-7}[\sim 43\% \text{M}] \rightarrow \beta\text{-L}[\sim 46\% \text{M}]$ (54%)	<i>d-d</i> transition
2.50	495	0.0274	$\beta\text{-H-6}[\sim 84\% \text{L}] \rightarrow \beta\text{-L}[\sim 46\% \text{M}]$ (10%)	LMCT involving amide \rightarrow metal
			$\beta\text{-H-2}[\sim 96\% \text{L}] \rightarrow \beta\text{-L}[\sim 46\% \text{M}]$ (15%)	LMCT involving phenyl ring attached to amide \rightarrow metal
			$\beta\text{-H}[\sim 97\% \text{L}] \rightarrow \beta\text{-L}[\sim 46\% \text{M}]$ (36%)	LMCT involving amide and phenyl ring attached to amide \rightarrow metal
3.36	369	0.0608	$\alpha\text{-H-1}[\sim 97\% \text{L}] \rightarrow \alpha\text{-L+1}[\sim 99\% \text{L}]$ (38%)	Intraligand Charge transfer between amide \rightarrow pyridine
			$\beta\text{-H-1}[\sim 97\% \text{L}] \rightarrow \beta\text{-L+2}[\sim 99\% \text{L}]$ (40%)	Intraligand Charge transfer between amide and phenyl ring attached to amide \rightarrow pyridine
3.86	321	0.0533	$\alpha\text{-H-1}[\sim 97\% \text{L}] \rightarrow \alpha\text{-L+2}[\sim 99\% \text{L}]$ (15%)	Intraligand Charge transfer between amide and phenyl ring attached to amide \rightarrow pyridine
			$\beta\text{-H}[\sim 97\% \text{L}] \rightarrow \beta\text{-L+3}[\sim 98\% \text{L}]$ (13%)	Intraligand Charge transfer between amide and phenyl ring attached to amide \rightarrow pyridine
			$\beta\text{-H}[\sim 97\% \text{L}] \rightarrow \beta\text{-L+4}[\sim 100\% \text{L}]$ (22%)	Intraligand Charge transfer between amide and phenyl ring attached to amide \rightarrow pyridine

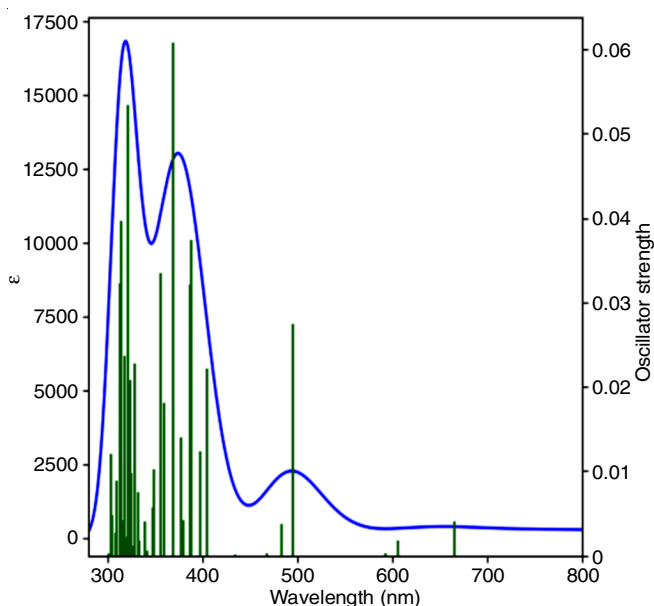


Fig. 5. TD-DFT calculated electronic spectrum for $[\text{Cu}(\text{II})\text{L}_2]$

FT-IR studies: The experimental FT-IR spectrum of $[\text{Cu}(\text{II})\text{L}_2]$ was recorded in the region $4000\text{--}400\text{ cm}^{-1}$ (Fig. 6a). Theoretically harmonic vibrational frequencies of the same were also calculated (Fig. 6b). The calculated frequencies were in a comparable agreement with the experimental frequencies and also with the reported results [13]. For example; C-H vibrations: generally aromatic C-H vibrations were observed in the region $3150\text{--}3000\text{ cm}^{-1}$. In present case, the experimental and theoretical values were 3165 and 3190 cm^{-1} , respectively, aliphatic C-H vibrations were observed in the region of $3000\text{--}2840\text{ cm}^{-1}$. In $[\text{Cu}(\text{II})\text{L}_2]$ complex, the asymmetric C-H stretching frequency has the experimental and theoretical values of 3070 and 3094 cm^{-1} , respectively whereas the symmetric C-H stretching frequency has the experimental and theoretical values of 3015 and 3014 cm^{-1} , respectively. The C=O vibrations are generally observed in the region of $1650\text{--}1810\text{ cm}^{-1}$. In present case, $[\text{Cu}(\text{II})\text{L}_2]$ complex has two C=O moieties in two different ligands bound to Cu(II) ions. One has the experimental and theoretical values of 1665 and 1676 cm^{-1} , respectively and the other has the values of 1636 and 1644 cm^{-1} , respectively. All such vibrations have been enlisted in Table-3. In total, 162 vibrational modes were obtained upon calculation, among them 24 vibrations with maximum intensities are displayed.

TABLE-3
EXPERIMENTAL AND COMPUTATIONAL CAL. VIBRATIONAL WAVENUMBERS [HARMONIC FREQUENCY (cm^{-1})]

S. No.	Exp. (cm^{-1})	Calculated wavenumber (cm^{-1})	IR intensity	Vibrational assignment
1	3273	3257	5	
2	3224	3216	7	
3	3165	3190	32	$\nu(\text{C-H})$ aromatic
4	3070	3094	25	$\nu_{\text{as}}(\text{C-H in CH}_3)$
5	3015	3014	46	$\nu_{\text{s}}(\text{C-H in CH}_3)$
6	1692	1678	62	
7	1665	1676	393	$\nu(\text{C=O})$
8	1650	1647	30	
9	1636	1644	238	$\nu(\text{C=O})$
10	1618	1626	75	
11	1605	1622	46	
12	1525	1520	390	$\nu(\text{C}_{\text{aromatic ring}}=\text{C}_{\text{aromatic ring}})$
13	1485	1484	41	
14	1472	1473	39	
15	1391	1380	320	$\nu_{\text{s}}(\text{C-N}_{\text{amide}})$
16	1365	1356	120	
17	1324	1330	60	
18	1300	1297	25	
19	1273	1270	192	$\nu(\text{C}_{\text{ether/aryl ring}}-\text{O})$
20	1251	1246	103	$\nu(\text{C}_{\text{methyl group}}-\text{O})$
21	1065	1056	70	$\nu(\text{C-H})$ (in plane bending)
22	954	950	43	
23	780	785	32	$\nu(\text{C-H})$ (out-of-plane bending)
24	772	767	52	

Conclusion

In summary, DFT calculations and experimental studies were performed on Cu(II) complex of a deprotonated pyridine amide ligand with appended ether functionality $[\text{Cu}(\text{II})\text{N}_{(\text{amide})_2}\text{N}_{(\text{pyridine})_2}\text{O}_{(\text{ether})_2}]$. The present investigation helps us to correlate the calculated theoretical findings and available experimental data. Minor discrepancies between observed and theoretical values were identified in each case, which could be attributed to the fact that the calculations were actually performed for a single discrete molecule. On the other hand, the experimental data obtained in the solid/liquid state are the bulk properties of the complex. Hence, present findings with only reasonable/ignorable deviations from the experimental values must be correct.

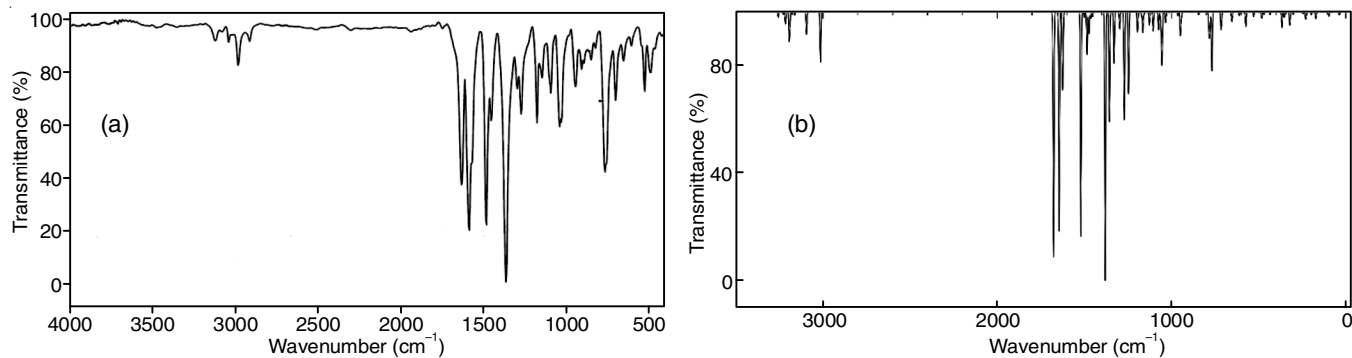


Fig. 6. (a) Experimental and (b) Theoretical FT-IR spectrum for $[\text{Cu}(\text{II})\text{L}_2]$

CONFLICT OF INTEREST

The authors declare that there is no conflict of interests regarding the publication of this article.

REFERENCES

1. S. Mahesh, K.-C. Tang and M. Raj, *Molecules*, **23**, 2615 (2018); <https://doi.org/10.3390/molecules23102615>
2. R. Chandra Maji, S. Mishra, A. Bhandari, R. Singh, M.M. Olmstead and A.K. Patra, *Inorg. Chem.*, **57**, 1550 (2018); <https://doi.org/10.1021/acs.inorgchem.7b02897>
3. A. Sengupta, A. Rajput, S.K. Barman and R. Mukherjee, *Dalton Trans.*, **46**, 11291 (2017); <https://doi.org/10.1039/C7DT01577A>
4. O. Belda and C. Moberg, *Coord. Chem. Rev.*, **249**, 727 (2005); <https://doi.org/10.1016/j.ccr.2004.08.025>
5. A. Rajput and R. Mukherjee, *Coord. Chem. Rev.*, **257**, 350 (2013); <https://doi.org/10.1016/j.ccr.2012.03.024>
6. T.C. Harrop and P.K. Mascharak, *Acc. Chem. Res.*, **37**, 253 (2004); <https://doi.org/10.1021/ar030153z>
7. P. Kumar and R. Gupta, *Dalton Trans.*, **45**, 18769 (2016); <https://doi.org/10.1039/C6DT03578G>
8. M. Amirnasr, M. Rasouli and K. Mereiter, *J. Iran. Chem. Soc.*, **10**, 275 (2013); <https://doi.org/10.1007/s13738-012-0156-6>
9. M. Eckshtain-Levi, M. Orio, R. Lavi and L. Benisvy, *Dalton Trans.*, **42**, 13323 (2013); <https://doi.org/10.1039/c3dt51543e>
10. B. Mondal, B. Sen, E. Zangrando and P. Chattopadhyay, *J. Chem. Sci.*, **127**, 1747 (2015); <https://doi.org/10.1007/s12039-015-0954-3>
11. A.K. Patra, M. Ray and R. Mukherjee, *Polyhedron*, **19**, 1423 (2000); [https://doi.org/10.1016/S0277-5387\(00\)00390-9](https://doi.org/10.1016/S0277-5387(00)00390-9)
12. S. Kumar and R. Gupta, *Indian J. Chem.*, **50A**, 1369 (2011).
13. F.A. Alseroury, *Aust. J. Basic Appl. Sci.*, **5**, 611 (2011).